Characterisation of small defects using miniaturised EMAT system

O. Trushkevych, R. S. Edwards

Department of Physics, University of Warwick, Coventry CV4 7AL, United Kingdom

Abstract

Many surface breaking defects, such as those caused by thermal fatigue or stress corrosion, have finite lateral dimensions. However, much of the research considers significantly larger simulated defects. This paper considers defects with mm-dimensions, and presents a method for characterisation of their length and depth. This is done using non-contact ultrasonic techniques, including a pair of electromagnetic acoustic transducers (EMATs) with significantly reduced size compared to standard industrial EMATs. Defects with dimensions of 1–11 mm length and 0.5–2 mm depth are measured. All information is obtained from a single raster scan of a sample, considering transmission and enhancement of Rayleigh waves, and introducing the defect cross-section. The lateral size resolution for the scan steps chosen is ±1 mm, and depth resolution is ±0.5 mm. The method, being non-contact, is also demonstrated on a sample with a 110 μm thick coating.

Keywords: Ultrasonics, EMAT, Rayleigh wave, Small defects

1. Introduction

Ultrasound is a powerful tool for detection and characterisation of defects. Research typically uses simulated defects which are large compared to the transducer under test; however, most real surface-breaking cracks have finite lateral dimensions. The sizes of interest depend on the particular application; typical lengths for surface-breaking defects may be 1–10 mm or smaller. Methods that are routinely used to characterise such small surface cracks include dye penetrant testing and magnetic particle inspection [1–3]. These can require the removal of any coating prior to inspection, which is potentially costly and environmentally unfriendly, and the inspection may contaminate the sample. An alternative is to use eddy current inspection, which is well-suited to detecting surface defects on conductive materials and components, including through thin non-conductive coatings [1, 4, 5]. Inspection is limited near sample edges, and magnetic permeability changes as well as lift-off variations are sources of noise [6–9]. Extracting defect depth from eddy current testing is possible, but can require complex processing [4, 10–13].

Phased array ultrasonic techniques give excellent sizing and resolution for small defects which are in a suitable location within the sample [14, 15], but require contact with the sample and the use of couplant. Coatings can complicate interpretation of results or block signals completely. Electromagnetic acoustic transducers (EMATs) can generate and detect ultrasound on electrically conducting and/or magnetostrictive materials, with operation possible through some coatings, and no couplant required [16, 17]. The coating should have low conductivity, and coating thickness or liftoff of the EMAT above the sample surface is limited to a few mm. The lift-off which can be obtained depends on the EMAT design, the frequency of inspection, and

Email address: r.s.edwards@warwick.ac.uk (R. S. Edwards)

sample conductivity. However, the size of the EMATs is typically large compared to the defect sizes of interest here, giving difficulties with spatial resolution.

EMATs are well suited for generating and detecting surface acoustic waves such as Rayleigh waves, which are useful for inspection of defects on the same side of the sample as the transducers. Previous work has shown that surface breaking defects can be analysed using both far-field and near-field techniques [18–20]. When a crack-like defect is significantly longer than the EMAT detector, it is common to calibrate transmission with different defect depths to enable defect sizing [18, 19, 21]. In addition, in the near-field of the defect the constructive interference of incident, reflected and mode-converted waves gives an increase in the signal [18]. The ratio of the enhanced amplitude to the incident amplitude is the enhancement factor, F_E. These factors are different for in-plane (IP) and out-of-plane (OP) components of the wave due to the differences in mode conversion and wave behaviour at the defect. The ratio between the IP and OP enhancements can be analysed to give the angle of crack propagation relative to the surface normal [18]. When used alongside measurement of the frequency-dependent transmission, long length surface-breaking cracks can be fully characterised.

Industrially produced EMATs are typically around 25–50 mm in lateral dimensions, as a large coil and magnet will give a large signal amplitude. However, for a defect which has lateral dimensions which are smaller than those of the detector, only part of the wavefront will interact with the defect. A schematic of this is shown in figure 1 for two different defect sizes. As the defect length becomes of the order of or smaller than the EMAT coil, measured transmission will increase due to waves passing around the defect edges. In addition, the measured signal enhancement will be an average over the region containing the defect, where constructive interference gives an increased amplitude, and neighbouring areas that produce no enhancement, and will hence be reduced.

One method to improve resolution is to use focused EMATs, producing a mm-dimension focal point [24, 25]. This paper uses an alternative technique, where small lateral dimension defects (called throughout the paper *small length*) are characterised using a detector with lateral size significantly smaller than standard EMATs. This comes with a corresponding drop in signal to noise ratio (SNR), but offers a compromise between resolution and scanning speed. The paper discusses the analysis used, considering transmission and enhancement. The defect cross-section is introduced and used alongside two-dimensional (2D) scans to size the surface length of the defect. An additional dimension of *crack length* is introduced in order to choose a suitable depth calibration. This technique offers the potential for sizing defects under coatings, where the crack length is not always straightforward to measure.

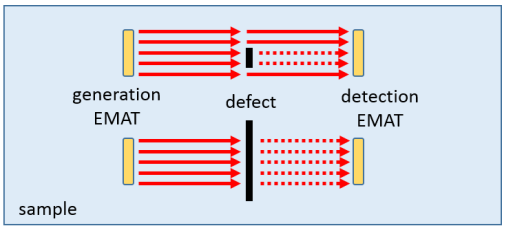

Figure 1: EMAT length compared to defect length.

Rayleigh wave interaction with wide defects (larger than the EMAT length) has been modelled in the literature, with a similar setup to this work modelled in reference [18] considering detection of IP and OP velocity components. In this paper we focus on experimental demonstration of EMAT miniaturisation, obtaining suitable SNR and characterising small cracks through coatings, based on the understanding of Rayleigh wave interaction with wide defects from the literature.

2. Experimental details

Aluminium blocks of sufficient thickness to support a Rayleigh wave (over 50mm thickness) were prepared by removing the top 3 mm layer [30]. This is a standard procedure and ensures any variation in anisotropy and residual stress due to the methods used in producing the bars (rolling) is removed. Two sets of samples were produced. For the first, slots of depths between 0.25 mm and 20 mm were ma-

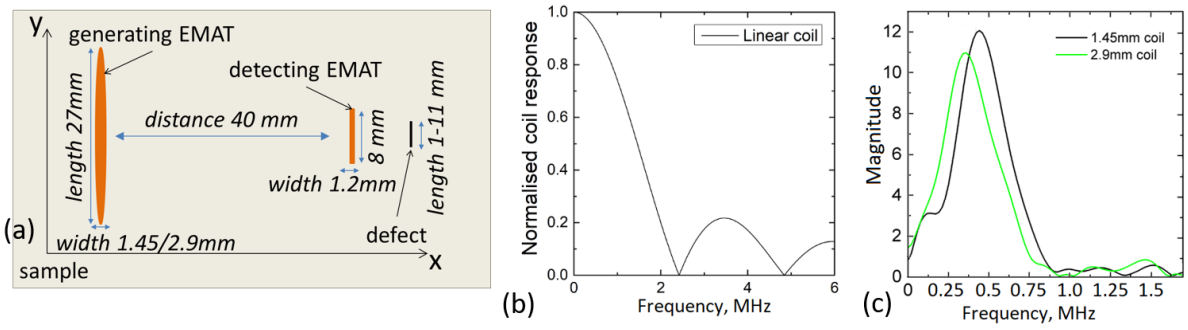

Figure 2: (a) Schematic of the EMAT scanning system; (b) Calculated frequency sensitivity of the detection coil [26]; (c) Frequency content of Rayleigh wave generated on an aluminium block.

chined across the full width of the block. Additional samples were produced containing slots with lengths ranging from 1 to 11 mm in 2 mm increments, and with depths of 0.5, 1, 1.5 and 2 mm, giving a total of 24 non-full-width slot defects. The defect width (opening of the slots) was 0.3 mm.

Figure 2(a) shows the experimental set-up adopted for the measurements. A generation and detection EMAT were used in a pitch-catch arrangement and scanned over the sample. Measurements were done using a 2D raster scan, whereby the EMATs were held with a fixed separation then scanned in the x-direction, then moved a set distance in the y-direction before another x-scan. An EMAT pulser designed and built in-house was used, with detected signals recorded using an oscilloscope and a LabVIEW scanning routine.

Careful consideration of EMAT design is essential to enable improved spatial resolution without risking significant loss of SNR as the EMAT sizes (magnet and coil) are reduced. The signal reduction depends on factors including coil and magnet size, sample material, and lift-off, but the primary requirement is to obtain sufficient SNR to enable analysis of the signals as the other factors will be constant during a scan. The most commonly used design for an EMAT detector is a linear coil wound around a magnet. To analyse small cracks, the detector coil length was set as 8 mm, comparable to the crack lengths (figure 2(a)). The magnetic field direction used determines the velocity component (IP or OP) which the detector will be primarily sensitive to [16, 18, 28]. EMATs were produced to measure both components. The detection EMAT coils were produced by hand-winding a 1.2mm wide coil using 0.08 mm diameter wire around the centre of a cuboidal magnet with side lengths of 8 mm, giving a coil length which matched the magnet dimensions. The field direction was chosen to be sensitive to predominantly the IP or OP velocity component citeRosli12.

The physical properties of the coil (length, width, number of turns) affect detection. A wide detection coil with many turns will cover a large area of the sample and provides good SNR. However, the sensitivity of the coil to different wavelengths is dependent on coil width, with a wider coil having a lower cut-off frequency [26, 27]. The expected frequency sensitivity of the 1.2 mm wide detection coil is shown in figure 2(b).

Racetrack coils were used to generate ultrasound. Coil miniaturisation and the use of the racetrack coil design, over a linear coil, allows for significant reduction of circuit inductance [27]. This in turn reduces the dead-time related to the EMAT and amplifier response, during which no signals can be measured. This allows one to bring the generator and detector closer together, reducing wave attenuation and increasing SNR. Ferrite enhanced generation (magnet-free) was used to improve lift-off performance and simplify scanning on magnetic samples [29]. The length of the generation coil was 27 mm, so that the wavefront arriving at the detector was close to pla-

gen. coil width	λ_R	λ range
1.45 mm	6.5 mm	3.2 – 10.3 mm
2.9 mm	8 mm	3.8 – 15 mm

Table 1: Wavelength content of the Rayleigh waves generated by each coil on an aluminium sample. λ_R is the central wavelength.

nar. Two generation coils of widths 1.45 and 2.9 mm were tested, as the coil width influences the wavelength of the generated ultrasound. The excitation current pulse width could be tuned from 300 ns to 2 μs. The width was chosen to maximise the amplitude of the generated Rayleigh wave and was in the region of 1.5 μs. The fast Fourier transform (FFT) of the signals obtained with each are shown in figure 2(c). The frequencies obtained are dependent on the sound velocity in the sample, generation and detection EMAT parameters (dimensions, designs), and excitation signal used. The wavelength distribution for generation-detection EMAT system in case of both generation coils on an aluminium block is summarised in figure 2(c) and table 1.

3. Results

3.1. Scans using miniaturised EMAT system

Figure 3 shows typical data obtained using this experimental configuration for an 11 mm long, 1.5 mm deep slot, plotting the IP velocity measurement. Figure 3(a) shows a B-scan, obtained by scanning the EMATs along the x-direction, with the EMATs aligned with the defect centre. The Rayleigh wave peak-to-peak amplitude was extracted at each position, and plotted in figure 3(b). Transmission T, and enhancement F_E, were extracted from the amplitude levels (A) defined in figure 3(b);

$$T = \frac{A_{transmitted}}{A_{incident}}; \qquad F_E = \frac{A_{enhanced}}{A_{incident}}. \qquad (1)$$

Figure 3(c) shows a full Rayleigh wave amplitude map. This was built during a 2D raster scan for y-steps of 1 mm, plotting the measured amplitude of the Rayleigh wave at each position as a colour. The image was produced using Igor software, which

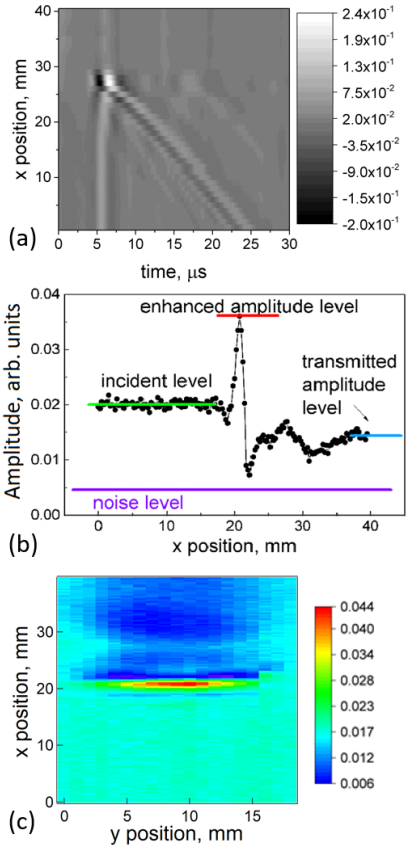

Figure 3: (a) B-scan produced during a single x-direction scan; colour represents wave amplitude. (b) Maximum amplitude of the Rayleigh wave at each position in the scan. (c) 2D map produced by plotting the amplitude at each position in a raster scan. 11 mm wide, 1.5 mm deep slot, IP component.

does not perform any smoothing of the data. The green region shows the constant amplitude prior to the EMATs reaching the defect. The red and dark blue horizontal lines show constructive and destructive interference at the defect as the detection EMAT passes over the defect. The pale blue region represents a drop in amplitude after the detection EMAT has passed over the defect and the signals are partially blocked. The SNR for the raster scan was calculated from the line scans for an undamaged part of the aluminium block. This takes into account not only EMAT signal amplitude but also lift-off variations and other noise contributions during a scan.

SNR was 119 for the IP component and 5 for the OP component.

3.2. Transmission calibration

Changes in transmission for full-width cracks have been used to gauge their depth [18]. However, for cracks which are not the entire width of the sample, the transmission will depend on crack length. Measurements were done for all full-width and small length slots, with the scan in the x-direction and performed with the EMATs symmetrical about the centre of the narrow slots. Standard deviation was calculated on all calibration values based on three repeated measurements. The transmission calibration results are expected to differ slightly for the two generation coils as the energy of a Rayleigh wave is primarily within one wavelength of the sample surface [31].

Figure 4(a) shows the transmission for full-width slots. The near-exponential drop as the defect depth increases follows results reported previously, with the drop with depth dependent on the frequency content in the pulse [18]. Figure 4(b) and (c) show the transmission as a function of defect length for different depth defects for the two generation coils. Transmission is well-suited for sizing defects deeper than 1 mm and longer than 5 mm for the Rayleigh wave frequency content used here, as clearly measurable changes are observed. On very shallow and small length defects transmission is not a sensitive tool, but this could be improved by using higher frequencies and smaller EMATs. As the defect length increases the transmission drops, heading towards the full-width value, with some diffraction occurring around the defect even when it is of a similar size to the detection EMAT. A measurement of defect length is required before the transmission calibration can be used, to avoid underestimation of depth.

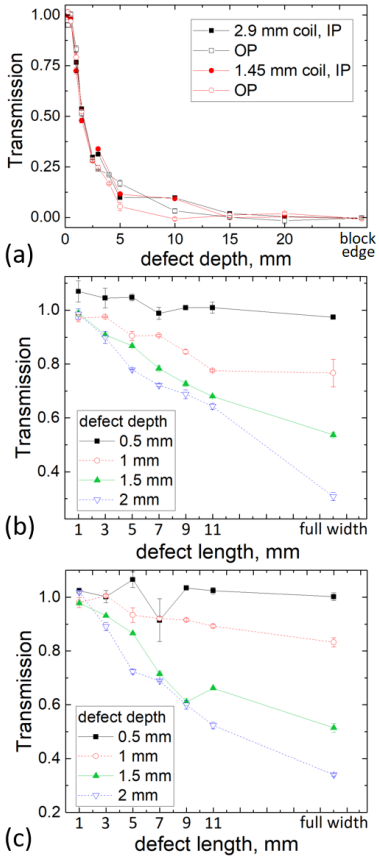

Figure 4: Transmission of Rayleigh waves for two generation EMATs. (a) full width slots; (b) & (c) small length slots.

3.3. Lateral detector size

The lateral size of an EMAT detector is not considered for large, commercial EMAT coils and large defects, as any effect due to a change in efficiency of detection at the edges of the coil is negligible. However, as the coil and defects become smaller in length, one must consider how much of the coil area is actively contributing to detection so that the effect of the smaller coil and crack lengths can be accounted for.

The magnetic field for the detection coil does not point directly into or parallel to the surface normal close to the magnet edges. Therefore the full extent of the EMAT coil will not be efficient for detection of the chosen velocity component, and the effective size of the EMAT needs to be determined. A scan of a sample edge (infinite depth crack) with finite lateral dimensions was used to determine effective coil length. The sample was an aluminium block with a section removed, and is shown schematically along with the scan details in figure 5(a). The EMATs were scanned with 0.25 mm steps along the x-direction

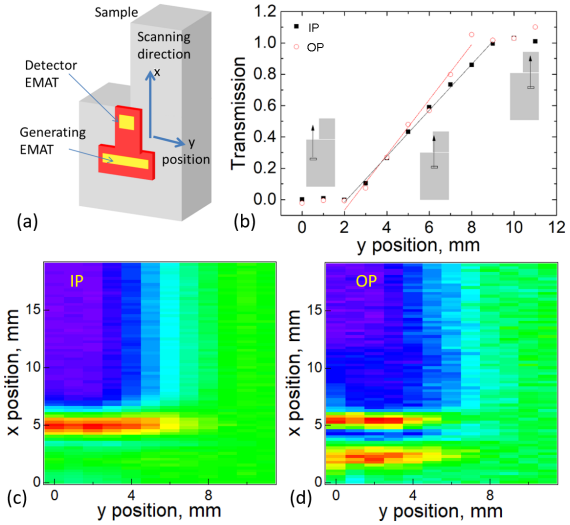

Figure 5: Transmission of Rayleigh wave by infinite depth crack with finite lateral dimensions. (a) Sample and scan schematic; (b) transmission, (c) scan map, IP component; (d) scan map, OP component.

and 1 mm steps in the y-direction, producing the full maps for the corresponding components shown in figures 5(c)&(d). As before, green or yellow on the colour scale corresponds to full transmission, red corresponds to signal enhancement (larger amplitude), and blue corresponds to destructive interference and partial / full blocking of the signal. The change from light blue to dark blue (no signal) is clear on both scan maps as the detection EMAT moves from being fully on to being fully off the sample as y is changed.

Transmission measured at a value of x such that the EMATs are on either side of the removed section (or at an equivalent x position over the section of the sample which remains whole) is plotted as a function of y-position in figure 5(b). This shows the zero transmission region when the detection EMAT is fully off the sample, the full transmission region when the detection EMAT remains fully on the sample, and the transition region in-between where the detection EMAT is partially on the sample.

Fitting the slope of the transition region in figure 5(b) (where transmission changes from 0 to 1) by a linear function $f = kx$ (with $k = 1/(x_1 - x_0)$), and taking the inverse of k, allows one to obtain a more precise measurement of the width of the transition region $(x_1 - x_0)$, with the coordinates specifying the start and end of efficient detection. This corresponds to the apparent width of the sensor. The slopes are different for IP and OP sensors of the same dimensions due to the curvature of the magnetic field at the coil edges [18]. For detection primarily of the IP velocity component, the effective detector length was calculated to be 7.6 mm. For the primarily OP velocity component detector it was 6.5 mm, with the remainder of the coil being ineffective for significant amplitude detection. This EMAT characterisation is essential for later defect sizing.

3.4. Signal enhancements

Choice of a suitable transmission calibration requires knowledge of the defect length. For a sample where visual inspection can be performed this can be straightforward; however, for defects under coatings removal of the coating or another method is required. Defect length can be extracted directly from the signal enhancement measured during a 2D scan, when the effective detector length is known. Once this information is available, defect depth can be obtained.

Figure 6 shows 2D scans (IP) of different length 1.5 mm deep defects. The region of enhancement (red/yellow horizontal line) has a different size for different length cracks. Because this is a 2D scan, smaller defects will show as a wider, lower amplitude enhancement due to the signal being averaged over areas with or without enhancement. The length of the enhancement is governed by the positions where the defect interacts with part of the coil (see figure 1). All defects will show a smooth decay to the enhancement at the edges as the EMAT detector moves partially off the defect.

Figure 7(a) shows the EMAT and defect cross sections. For this work, s is the effective detector length, l is the defect length, and d is the defect depth. As the EMAT passes over the defect, the measured enhancement will increase from 1 (no enhancement) to its maximum value. Once the EMAT is fully over the defect it will record a constant enhancement, with the size of the enhancement dependent on the length and depth of the crack. When the EMAT starts to leave

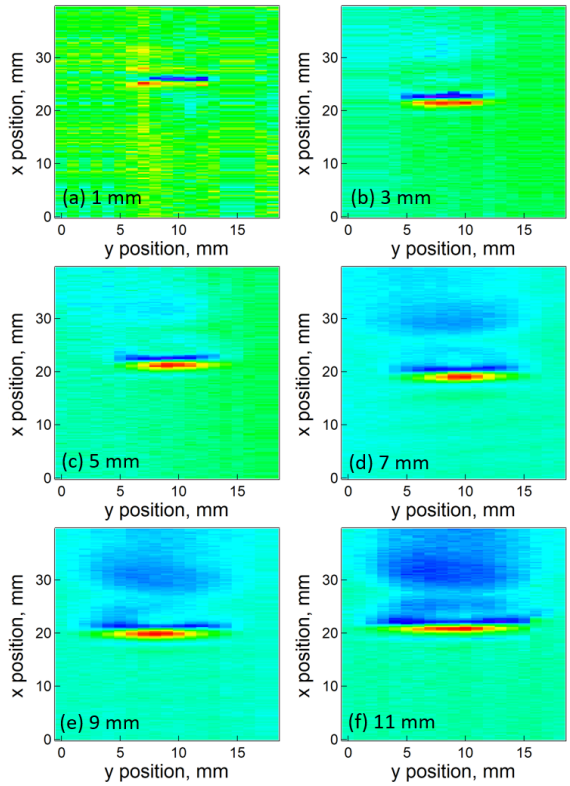

Figure 6: Scan maps of 1.5 mm deep cracks of varying length: a)1 mm; b) 3 mm; c) 5 mm; d) 7 mm; e) 9 mm; f) 11 mm; IP data, 2.9 mm generation coil. The colours cover the same detected voltage range in all images.

the other side of the crack, a corresponding drop in enhancement is observed.

For short length defects where $l < s$, shown in figure 7(b), the region over which the signal enhancement increases to its maximum value is given by the crack length, l. The region over which the signal is at a maximum is $s - l$. In contrast, for longer length defects where $l > s$, shown in figure 7(c), the region over which the signal enhancement increases is the detector length s, and the central region has a length of $l - s$.

The length over which the defect is detectable using the enhancement (*apparent crack length*, L) is measured from the image produced during a scan, or from taking a line of data out at a value of x at which the enhancement is measurable. Examples of this are shown in figure 8. Should a measurement of the apparent length L be taken from measuring where the enhancement simply increases above 1 (no enhancement, shown as the axis in the schematics in figure 7), ignoring any noise effects, the length over which the defect will be measured is $L = l + s$. However, in practice one must define a threshold above which a defect is recorded, to allow for noise. This has the effect of reducing the apparent length, as shown in figure 7(d), giving an apparent length of

$$L = l + s - 2\Delta. \tag{2}$$

Δ is an experimentally derived property which is linked to the minimum detectable defect length and depth for the chosen EMAT and frequencies of operation, and the threshold level. Should the measured enhancement when the EMAT is fully over a defect just reach the threshold level, then $\Delta = l$, the length of this defect. The shortest or shallowest detectable defect with a length l_{min} will have an enhancement which just reaches this threshold level, before immediately decaying as the EMAT moves off the defect, and hence $\Delta = l_{min}$. For the EMATs and frequencies used in this research the minimum detectable defect was 1 mm long and 0.5 mm deep (measured using a caliper with 0.1mm precision), giving a value for $\Delta = 1$ mm for these measurements. In practice, there will also be errors on the value for L associated with the step size used in the scanning, giving an over- or under-estimate of the length.

Figure 8 shows how the Rayleigh wave enhancements in the 2D scan maps in figure 6 vary as a function of scan position in the y-direction, giving the profile of the enhancement behaviour. This is shown for IP and OP components for defects with the same depth (1.5 mm) and different lengths. For each defect the enhancement grows from 1 (no enhancement, crack is not detectable) to various values, with longer defects generally larger in the centre as the defect is closer in length to the detection coil. As the sensor passes over the other end of the defect the enhancement reduces back to 1.

The crack length l was measured using a set of calipers with ± 0.1 mm precision. It was also calculated from the L values obtained in the scans by

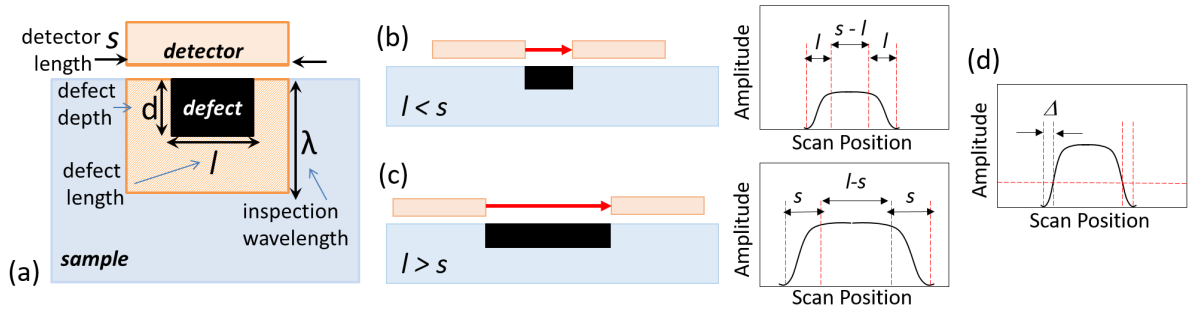

Figure 7: (a) Cross section of EMAT and defect. (b) and (c) show the scanning schematic and expected enhancements (x-axis is at $y = 1$) for $l < s$ and $l > s$. (d) shows the effect of adding a threshold (horizontal dashed line).

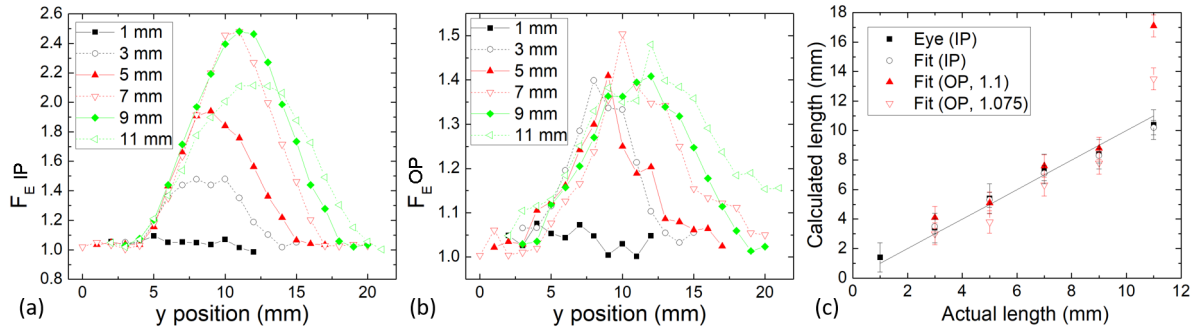

Figure 8: Enhancements across 1.5 mm deep cracks of varying length: (a) IP enhancement; (b) OP enhancement, (c) measured lengths, all for 2.9 mm generation coil.

using equation 2, as summarised in table 2. The region from the 2D map containing enhancements was extracted as in figure 8. L was calculated using several methods; measurement by eye (regions with enhancement, allowing for consideration of noisy signals for small defects where thresholding is not appropriate), and fitting of a Gaussian to the enhancements data and applying a threshold. For the IP data the threshold was set as 1.1. For the OP data, which is typically much noisier ($\mathrm{SNR}_{OP} = 5$, $\mathrm{SNR}_{IP} = 119$), two thresholds were used. The scan step size was 1 mm, and a value of Δ of 1 mm is assumed; this corresponds to the minimum detectable defect length, which is linked to resolution, SNR, and scan step size, and is experimentally determined for the step size and EMAT dimensions. For these measurements it is dominated by step size. The value of s is 7.6 mm for the IP data and 6.5 mm for the OP data.

The agreement between calculated and actual values is very good. The precision on calculated length is sufficient for choosing a transmission calibration curve. Greater precision could be obtained with finer scan step sizes. Note that the OP measurements have a larger error due to lower SNR of the OP EMAT system. Data for the 1 mm length defect was noise dominated and could not be fitted.

The size of the enhancement depends on defect extent compared to the coil, the slot geometry, and the reflection coefficient, which varies with depth. Figure 9 shows the measured enhancements for different depth defects as a function of defect length, for both generation coils. The measured OP component overall has a lower amplitude than the IP component, and therefore is more prone to noise.

All enhancements show a general increase with increasing defect length, as expected. For smaller de-

$l_{caliper}$	L_{eye}	l_{eye}	$L_{IP(1.1)}$	$l_{IP(1.1)}$	$L_{OP(1.1)}$	$l_{OP(1.1)}$	$L_{OP(1.075)}$	$l_{OP,1.075)}$
1± 0.1	7±1	1±1	–	–	–	–	–	–
3 ±0.1	9±1	3±1	9.1±0.5	3.5±0.5	8.6±0.75	4.1±0.75	7.5±0.75	3±0.75
5 ±0.1	11±1	5±1	10.9±0.5	5.3±0.5	9.6±0.75	5.1±0.75	8.3±0.75	3.8±0.75
7 ±0.1	13±1	7±1	12.7±0.5	7.1±0.5	12.1±0.75	7.6±0.75	10.8±0.75	6.3±0.75
9 ±0.1	14±1	8±1	13.9±0.5	8.3±0.5	13.3±0.75	8.8±0.75	12.3±0.75	7.8±0.75
11 ±0.1	16±1	10±1	15.8±0.5	10.2±0.5	21.6±0.75	17.1±0.75	18±0.75	13.5±0.75

Table 2: Measuring crack length from IP component enhancements (figures 6 and 8). All measurements are in mm. The number in brackets is the threshold applied for analysis.

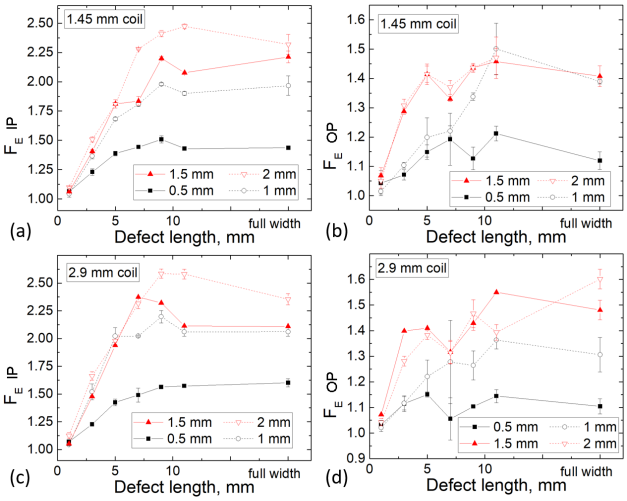

Figure 9: IP and OP enhancements for cracks of varying depth, plotted as a function of defect length, measured using both generation coils. (a), (c) IP enhancements; (b), (d) OP enhancements.

fects, the averaging effect underneath the coil causes a lower enhancement as parts of the coil see no enhancement. There is some variation of enhancement with depth. The IP component shows a general increase in depth, whereas for the OP component the 1.5 mm deep defects show a larger enhancement in places. This is due to the behaviour of the reflection coefficient R with depth [31]. This exhibits peaks at depths of around 0.2 and 0.5λ, and a dip at around 0.3λ. Waves reflected from defects with depths just above and below $d = 0.2\lambda$ (1.3 mm for the 1.45 mm generation coil, and 1.6 mm for the 2.9 mm coil) will have similar amplitudes and will hence produce similar enhancements; however, the signals are broadband and the measured enhancement will hence show averaging around these depths.

The enhancements shown in figure 9 offer the potential to be used as an additional calibration for finding defect depth. For a real defect a rough surface will affect the enhancements measured, but the ratio of the enhancement factors for the IP and OP should be affected similarly [18]. This calibration can be used in conjunction with the transmission calibration. The advantage of using enhancement alongside transmission is that there is a measurable change observed for smaller defects. If length is known, a measurement of T and F_E together will allow greater certainty on the depth measurement, allowing an increase in probability of detection and reliability of the sizes obtained.

3.5. Cross-section of Rayleigh wave interaction with a defect

The calibrations discussed above for transmission and enhancement can be very specific to a defect type [18], chosen EMAT pair (requiring knowledge of the exact frequency content), and sample. Should an EMAT need to be replaced, a new calibration may be required due to variations in production. A method that can offer flexibility for small changes and remove the requirement for frequent recalibration would be very beneficial. One method is to consider the defect cross section, which takes into account the central frequency of a broadband EMAT.

Detector footprint is defined as the area in the cross-section of the sample that the detector is sensitive to, and considers the approximate portion of the Rayleigh wavefront that the detector receives. It

is defined by the effective detector length s and the depth within which most of the Rayleigh wave energy is confined. The latter is set by taking the inspection wavelength λ (in practice, the central wavelength in the pulse is chosen). The *defect footprint* is the area of the crack that lies within the detector footprint area and therefore interacts with the Rayleigh wave. Figure 7(a) shows a schematic of the defect and detector footprints for the case where the defect is smaller than the detector.

The detector and defect footprints (areas) $S_{detector}$ and D_{defect} are defined as

$$S_{detector} = s\lambda; \qquad D_{defect} = l_{eff}d_{eff}$$
$$d_{eff} = \begin{cases} d, & \text{if } d < \lambda \\ \lambda, & \text{otherwise} \end{cases} \qquad l_{eff} = \begin{cases} l, & \text{if } l < s \\ s & \text{otherwise.} \end{cases} \tag{3}$$

The interaction cross-section σ is defined as the ratio of the defect footprint to the detector footprint,

$$\sigma = \frac{l_{eff}d_{eff}}{s\lambda}. \tag{4}$$

Limits must be placed on defect dimensions; for example, a defect which has a short length but large depth is not generally expected. The combined relationship between detector length and inspection wavelength, as well as the crack length and depth, are considered in this method.

Figure 10 shows the enhancement and transmission plotted as a function of defect cross-section for all defects measured, for two generation coils and considering IP and OP signals. Small cross section measurements were taken from the narrow width slots, while larger cross section measurements were done by using the full-width defects or a selected region with the EMATs partially off the sample, and hence are not as accurate. Also shown are exponential growth or decay fits for each coil.

The fits to the enhancements show that there are only small differences between the two coils; for the OP enhancements the fits are very close until the larger cross sections are reached. For the IP enhancements, the 1.45 mm coil has a consistently slightly smaller enhancement, but measurements are still very close for very small cross sections. There is a general growth in enhancement until a cross section of around 20%, followed by a leveling off of the signal. Hence this can be used as a method of sizing smaller cross-section defects. Despite the small differences between coils, there is a definite possibility for using this cross section method to give a measurement for a pair of similar but uncharacterised coils. This is important for hand-wound designs, where replacement of a broken transducer could require a check of the calibration.

Transmission shows a general decay as cross section increases. For the IP measurement, the two fits are near-identical, showing that the small frequency bandwidth differences between the two generation coils are not important here. There are larger differences between the two coils for the OP transmission, but this is primarily due to larger cross sections. This can be used in collaboration with the earlier transmission calibrations. One must consider that larger changes in transmission are easier to analyse than the very small changes at very small cross-sections.

The measurement of enhancement, with its sensitivity to cross sections lower than 20%, offers a sensible choice when analysing small defects. Using a combination of measurements will give a better accuracy in sizing; for example, a measurement of all four values plotted in figure 10 would give a cross-section from each measurement. The average cross-section can then be obtained, considering the importance and reliability of each measurement. Once cross-section is known, other measurements such as the 2D scan map can be used to identify defect length and hence obtain depth.

3.6. Characterisation of an unknown slot with and without coating

To test the capabilities of the methods, a slot in an aluminium block was tested with and without a 110 ± 1 μm layer of tape to mimic a coating such as a paint layer, with the slot dimensions unknown prior to testing. Adding a coating increases lift-off and will affect the central wavelength generated. This will affect the calibrations for transmission and enhancements, as well as decreasing the signal amplitude (in-

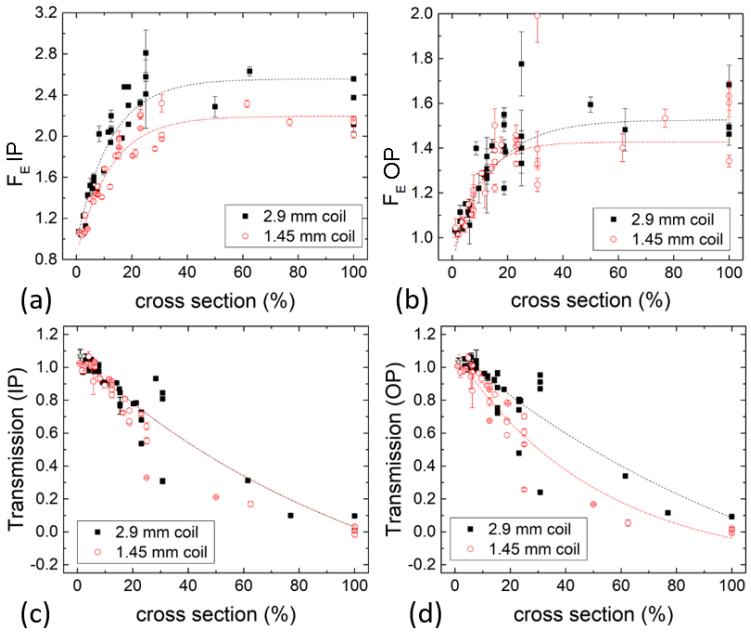

Figure 10: Enhancements and transmission for slots with varying length and depth as a function of interaction cross-section: Enhancement for (a) IP and (b) OP signals; transmission for (c) IP and (d) OP.

creasing SNR); scans are shown to demonstrate that cross-section is still calculable.

The generation coil with 1.45mm width was used. The 2D scan maps of IP and OP components are shown for the uncoated sample in figure 11(a) and (b), and for the sample with coating in figure 11(d) and (e). The OP component in both cases has a smaller amplitude and is hence more dominated. This is particularly noticeable in the coating scan, where there are several small regions with a higher signal which could signify a defect. However, the defect signal should show as an extended line, which is only present at the expected location, albeit with some variations across the line. To improve visualisation and reliability, figure 11(c) and (f) show the result of multiplying the two measurements together. The crack region is clear for both coating and no coating.

Measurement of the crack length was done by eye from the scan maps to give an indication of length, and by taking the profile of the signal amplitude across the crack and fitting to a Gaussian. The latter was used as the more reliable measurement of length. The scan maps show that the defect is small in length and depth, as indicated by the lack of blocking of the signal; this is confirmed by the transmission measurements which is close to one, and is therefore not used for sizing. The values for F_E are small but above 1, and hence are used alongside equation 2, giving crack length, to give crack depth. Two methods are used: calculation using the calibration from figure 9 (giving d_{cal}), and using the cross section fits from figure 10 (d_{cs}). All depth values extracted from the calibrations have ±0.5 mm error.

parameter		$l_{cal} \times d_{cal}$	$l_{cs} \times d_{cs}$
F_E^{IP}	1.28	1.8×2.3 mm	1.8×1.6 mm
F_E^{OP}	1.18	2.3×1.4 mm	2.3×1.6 mm

Table 3: Enhancements F_E for an uncoated slot in aluminium and the corresponding dimensions extracted from scan maps, enhancement calibrations and from cross-section calibration data.

Table 3 summarises the measurement results for

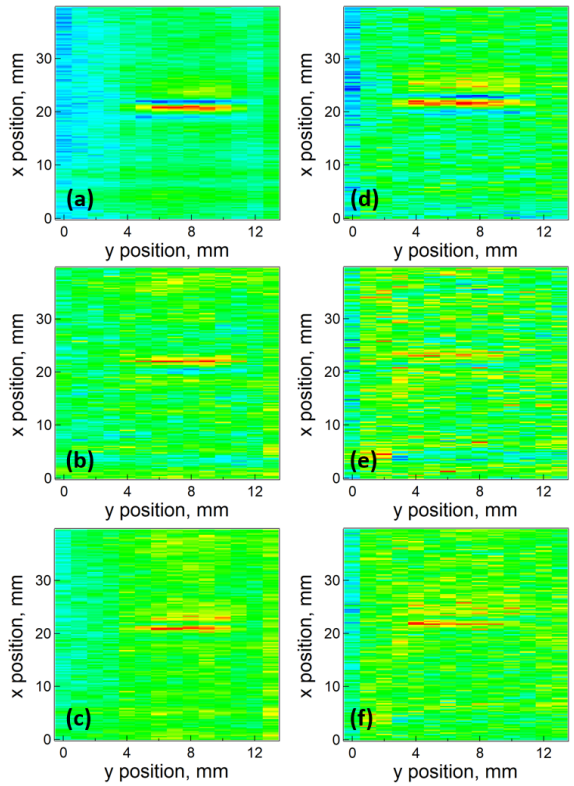

Figure 11: 2D maps of unknown slot; no coating, for (a) IP, (b) OP, (c) IP×OP; 110 μm coating, for (d) IP, (e) OP, (f) IP×OP.

the tests done without a coating. Assigning equal weight to all measurements and taking the average value, the measurements predict a defect of dimensions 2.05×1.7 mm, with an error of ±0.5 on each value. This is in excellent agreement with the true values, which were later measured using calipers to be 2 ± 0.1 mm wide and 1.5 ± 0.1 mm deep.

parameter		$l_{cal} \times d_{cal}$	$l_{cs} \times d_{cs}$
F_E^{IP}	1.18	2.9×0.8 mm	2.9×0.7 mm
F_E^{OP}	1.1	2.5×1.2 mm	2.5×1.1 mm

Table 4: Enhancements F_E for a coated slot in aluminium.

Table 4 gives the measured values for the coated sample. This gives an average size of 2.7×1.0 mm, with an error of 0.5 mm on each dimension. The results are more prone to noise given the higher lift-off, which leads to an over-estimate of the length and corresponding under-estimate of the depth. This is expected due to the spreading out of the wavefront, any damping effect that the coating may have on the Rayleigh wave, and reduction of magnetic field in the sample due to the lift-off. However, it is clearly possible to detect a small defect and analyze it through a 110 μm coating. An improvement to the accuracy could be obtained by re-testing at lift-off to give a more accurate value of Δ, which would take into account the spreading of the signal. It is likely that the minimum detectable defect size is larger, and this would lead to a corresponding reduction in the predicted lengths, and hence an increase in the calculated depths.

4. Conclusions

A miniaturised EMAT system has been developed and used to analyse defects with lengths which are comparable with the detector coil length, with resolution of smaller defects possible. Sizing a defect which is small in both length and depth through a thin coating from a single scan has been demonstrated, in contrast to earlier work which assumed a defect much larger than the coil dimensions. The effective detector length for EMATs which are primarily sensitive to either the IP or OP Rayleigh wave velocity component has been determined using a scan over an infinite depth defect with a finite length (block with L-shape) in order to identify the extent of the sensitivity of these EMATs. The frequency range and inspection wavelength have been chosen so that defects with depths of between 0.5 and 8 mm can be characterised in detail, with the main focus on defects up to 2 mm in depth.

Measurements have been done by performing 2D raster scans of samples to obtain full defect information. The lateral dimension of the defect as well as its depth can be obtained from a single raster scan by considering the transmission underneath and around the defect, the length of the enhancement region, and the cross-section measurement. The technique was demonstrated by characterising a small defect with

2 mm length and 1.5 mm depth, with and without a 110μm thick coating.

The efficiency of EMAT generation on other conducting industrial materials varies, and the system efficiency and SNR will depend on the material of the sample. If it is necessary to increase SNR, a magnet could be used instead of ferrite for generation, and larger magnets could be used for detection. However, where EMATs can be miniaturised and magnet size reduced, the reduced magnetic force between EMATs and the sample allow for easier scanning.

This technique offers an alternative to other methods for sizing surface-breaking defects, in particular where there is a coating in place. The scanning speed could be improved for on-line measurements by using a commercial scanning system and improvements to pulse repetition rate through advances in the electronics used to generate the ultrasound signals.

Acknowledgements

This work was funded by the ERC under the proof of concept grant 693243, NCUScan. The authors thank Robert Day for technical support.

References

[1] B. Purna Chandra Rao, Non-destructive Testing and Damage Detection, Springer Singapore, Singapore, 209–228 (2017).

[2] B. Larson, Study of the factors affecting the sensitivity of liquid penetrant inspections: Review of literature published from 1970 to 1998, Tech. rep., Center for aviation systems reliability (2002).

[3] D. Jiles, NDT & E International **23**(2) 83–92 (1990).

[4] G.Y. Tian and A. Sophian, NDT& E International **38**(1) 77–82 (2005).

[5] F. Hughes, R. Day, N. Tung and S. Dixon, Insight **58**(11) 596–600 (2016).

[6] Tian, G.Y.; Zhao, Z.X.; Baines, R.W. Sens. Actuat. A **69**, 148-151 (1998).

[7] Gui, Y.T.; Yong, L.; Mandache, C. IEEE Trans. Magn.**45**, 184-191 (2009).

[8] Theodoulidis, T.; Bowler, J.R. IEEE Trans. Magn. **46**, 1034-1042 (2010).

[9] Javier Garca-Martn, Jaime Gmez-Gil, Ernesto Vzquez-Snchez, Sensors **11**, 2525-2565 (2011).

[10] Yue Li ; L. Udpa ; S.S. Udpa IEEE Transactions on Magnetics, **40** , 2, 410 – 417 (2004).

[11] Bernieri, A., Ferrigno, L., Laracca, M., Molinara, M. IEEE Transactions on Instrumentation and Measurement, **57** ,9, 1958 – 1968 (2008).

[12] Ahmed, S., Miorelli, R., Salucci, M., Massa, A. Studies in Applied Electromagnetics and Mechanics: Electromagnetic Nondestructive Evaluation (XX), **42**, 228–235 (2017).

[13] Chaiba, S. A., Ayad, A., Ziani, D., Le Bihan, Y., Garcia, M. J. Journal of Nondestructive Evaluation, **37**, (3), 55 (2018).

[14] J. Cheng, J.N. Potter, A.J. Croxford and B.W. Drinkwater, Smart Materials and Structures **26**(5) 055006 (2017).

[15] M.V. Felice, A. Velichko, and P.D. Wilcox, NDT & E International **68** (Supplement C) 105–112 (2014).

[16] R.B. Thompson, Physical principles of measurements with EMAT transducers, Academic Press, 157–200 (1990).

[17] M. Hirao and H. Ogi, EMATs for science and industry. Noncontacting ultrasonic measurements., Kluwer Academic Publishers (2003).

[18] M. Rosli, R.S Edwards and Y. Fan, NDT&E international **49** 1–9 (2012).

[19] R.S. Edwards, B. Dutton, A.R. Clough and M.H. Rosli, Applied Physics Letters **99** 249901 (2011).

[20] A.R. Clough and R.S. Edwards, Journal of Applied Physics **111** 104906 (2012).

[21] B. Dutton, A.R. Clough, M.H. Rosli and R.S. Edwards, NDT & E International **44** 353–360 (2011).

[22] Y. Fan, S. Dixon, R.S. Edwards and X. Jian, NDT&E International **40** 471–477 (2007).

[23] R.S. Edwards, S. Dixon and X. Jian, NDT & E International **39(6)** 469–475 (2006).

[24] C.B. Thring, Y. Fan and R.S. Edwards, NDT&E International **81** 20–27 (2016).

[25] C.B. Thring, Y. Fan and R.S. Edwards, NDT&E International **88** 1–7 (2017).

[26] S. Dixon, S.E. Burrows, B. Dutton and Y. Fan, Ultrasonics **51** 7–16 (2011).

[27] C.B. Thring, S.J. Hill, S. Dixon and R.S. Edwards, submitted to Ultrasonics (2018).

[28] X. Jian, S. Dixon and R.S. Edwards, Insight **46**(11) 671–673 (2004).

[29] S. Dixon and X. Jian, Applied Physics Letters **89** 193503 (2006).

[30] S. Dixon, C. Edwards and S. Palmer, Insight **40**(9) 632–4 (1998).

[31] I.A. Viktorov, Rayleigh waves and Lamb waves - physical theory and application, New York: Plenum Press (1967).